

# Microstructure and microstructural evolution in BaTiO<sub>3</sub> films fabricated using the precursor method

L.A. Bendersky and C.J. Lu

Materials Science and Engineering Laboratory, National Institute of Standards and Technology, Gaithersburg, Maryland 20899

J.H. Scott

Chemical Science and Technology Laboratory, National Institute of Standards and Technology, Gaithersburg, Maryland 20899

K. Chang and I. Takeuchi

Department of Materials Science and Engineering and Center for Superconductivity Research, Department of Physics, University of Maryland, College Park, Maryland 20742

(Received 5 November 2001; accepted 24 June 2002)

Pulsed laser deposition of TiO<sub>2</sub> and BaF<sub>2</sub> layers at room temperature and subsequent annealing in flowing oxygen were used to form homogeneous epitaxial BaTiO<sub>3</sub> films on LaAlO<sub>3</sub>. This oxide film synthesis method, known as the precursor technique, is frequently used for making combinatorial libraries. In this paper, we investigated the microstructures of the films at different stages of annealing using cross-sectional transmission electron microscopy, high-resolution imaging, and electron energy loss spectroscopy. It was shown that epitaxial BaTiO<sub>3</sub> thin films with large grains could be formed on a LaAlO<sub>3</sub> substrate. Their formation process consists of the following stages: At 200 °C, the BaF<sub>2</sub> layer is partially oxidized. At 400 °C, the amorphous TiO<sub>2</sub> layer crystallizes, further transformation of BaF<sub>2</sub> into BaO takes place, and interdiffusion begins. At 700 °C, the formation of a polycrystalline structure with different Ba–Ti oxides occurs, epitaxial BaTiO<sub>3</sub> grains nucleate on the film/substrate interface, and significant interdiffusion takes place. Finally, at 900 °C, the interdiffusion is completed, and the epitaxial BaTiO<sub>3</sub> grains coalesce and grow. The presence of nonepitaxial polycrystalline regions in fully annealed films can be explained as the following: (i) stoichiometric transient regions not yet consumed by recrystallization of BaTiO<sub>3</sub>; (ii) nonstoichiometric regions resulting from inhomogeneous deposition of BaF<sub>2</sub>.

## I. INTRODUCTION

Combinatorial thin-film methods have recently been applied to exploring new and improved properties and compositions of different electronic materials.<sup>1,2</sup> In particular, the method was successfully used to improve and optimize properties of ferroelectric and dielectric oxide materials.<sup>3–6</sup> For example, using a discrete combinatorial library, it was found that W doping of (Ba,Sr)TiO<sub>3</sub> (BST) results in lower leakage current and lower microwave loss compared to the undoped BST.<sup>3,4</sup> Also Ba<sub>0.12–0.25</sub>Sr<sub>0.35–0.47</sub>Ca<sub>0.32–0.53</sub>TiO<sub>3</sub> was identified from a continuous composition spread of (Ba,Sr,Ca)TiO<sub>3</sub> as the compositional region with the lowest microwave loss.<sup>6</sup>

The central part of the methodology is the synthesis of *materials libraries* where on a single substrate a large number of different compositions, or a continuous spread

of compositions, are deposited. There are several different methods of creating a combinatorial library using thin-film deposition techniques. Precisely positioned shadow masks or automated shutters are used to control the amount of thin-film materials delivered to selected regions on a substrate. Different physical vapor deposition techniques can be used for this. In particular, pulsed laser deposition (PLD) has been successfully employed for oxide systems. The *precursor method* of combinatorial synthesis can truly bring out the combinatorial nature of the experimental approach. In this method, different compositions are created from combinations of amorphous precursor layers deposited at room temperature. By varying the combinations of precursors deposited at different positions, one can generate very diverse compositional variations across the libraries. In this method, following the depositions, libraries undergo controlled

thermal treatments to (i) diffuse and mix the precursors and (ii) crystallize an equilibrium compound at each site. One drawback of the precursor method is in the possibility of interfacial reaction with a substrate and, thus, the need to keep the temperature/time of annealing to a minimum. The lowered temperature may result in limited interdiffusion and, therefore, in incomplete mixing and formation of off-stoichiometric or metastable phases.

To understand the limit of the precursor technique for making libraries of oxides, it is important to investigate the details of the processes of mixing precursors and formation of phases. In this paper, we present results of detailed transmission electron microscopy (TEM) and electron energy loss spectroscopy (EELS) studies of single-composition BaTiO<sub>3</sub> (BTO) films made from BaF<sub>2</sub> and TiO<sub>2</sub> precursors deposited by PLD onto a (001) LaAlO<sub>3</sub> substrate. The room-temperature-deposited BTO films were annealed according to the optimized procedure,<sup>1,2</sup> and individual specimens processed up to different stages of the annealing were studied by cross-sectional TEM.

## II. EXPERIMENTAL

The BaF<sub>2</sub> and TiO<sub>2</sub> precursor films were deposited by PLD onto LaAlO<sub>3</sub> (LAO) substrates at room temperature in a vacuum of approximately 10<sup>-3</sup> Pa (approximately 10<sup>-5</sup> torr). The purities of the raw materials the manufacturer uses for TiO<sub>2</sub> and BaF<sub>2</sub> targets are 99.99% and 99.9%, respectively. The LAO substrate has pseudocubic [001] orientation. The TiO<sub>2</sub> layer was deposited first, followed by the deposition of the BaF<sub>2</sub> layer. The required thickness of the layers to be deposited was estimated according to the density and the molecular weight of the precursors. Typically we aimed to deposit approximately 130 nm of BaF<sub>2</sub> and approximately 70 nm of TiO<sub>2</sub>, respectively, so that the resulting annealed film would be approximately 200 nm of BaTiO<sub>3</sub>. We have found that the change in the total film thickness after the annealing processes is negligible.

After the deposition, the samples were first placed in a 200 °C oven for one week in ambient atmosphere. Following the 200 °C anneal, the samples were annealed at

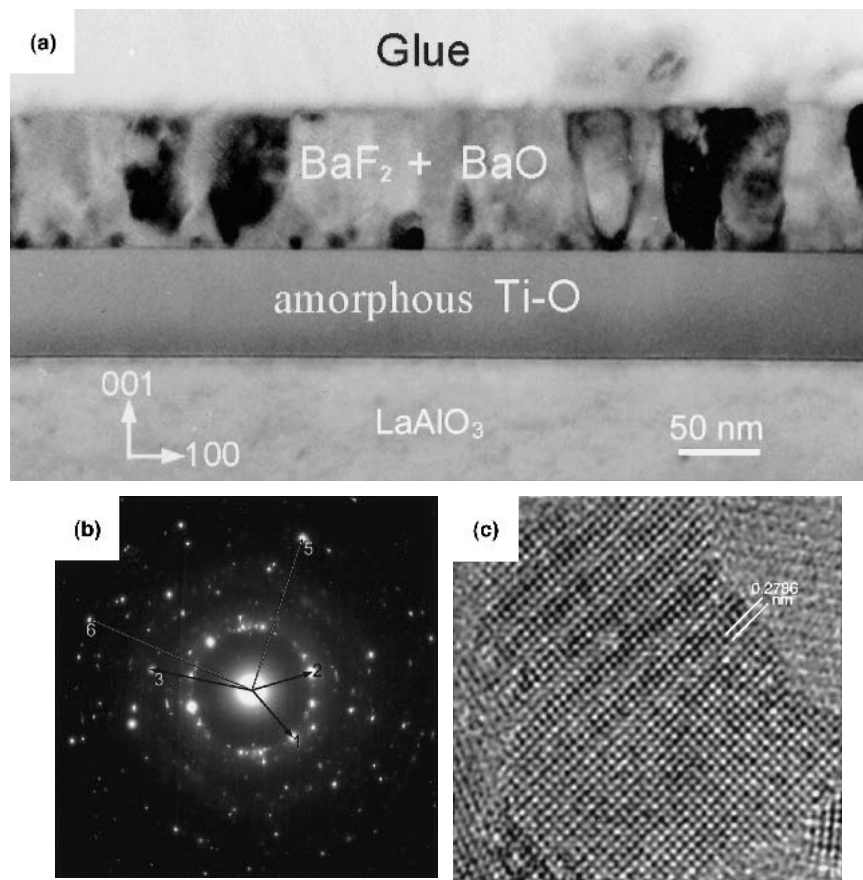


FIG. 1. (a) Cross-sectional TEM image of the BaF<sub>2</sub>/TiO<sub>2</sub> specimen annealed at 200 °C for one week. (b) SAED pattern obtained from an upper layer. (c) HREM image of a grain from the top layer. The phase contrast corresponds to the [100] zone axis of cubic BaF<sub>2</sub> fluorite. Periodic displacement of the image is a consequence of Moiré fringes coming from a slight overlap of grains.

400 °C for 24 h in flowing oxygen. Finally, the specimens were heated to 900 °C, annealed for 1.5 h, and cooled to room temperature in flowing oxygen. All the temperature ramps were done at 1 °C/min. A set of identically prepared samples was placed in the oven together. They were removed after different stages of the annealing process. Four specimens studied by TEM were taken out (a) after 200 °C annealing, (b) after 400 °C annealing, (c) after heating to 700 °C, and (d) after 900 °C annealing.

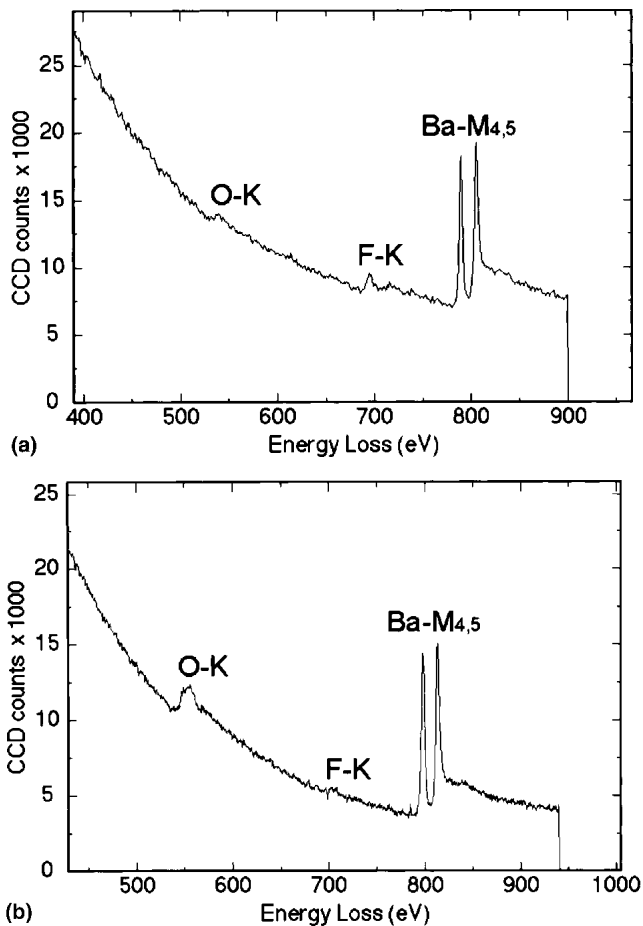


FIG. 2. EELS spectra from an upper part of a film acquired from the specimen annealed at (a) 200 °C and (b) 400 °C.

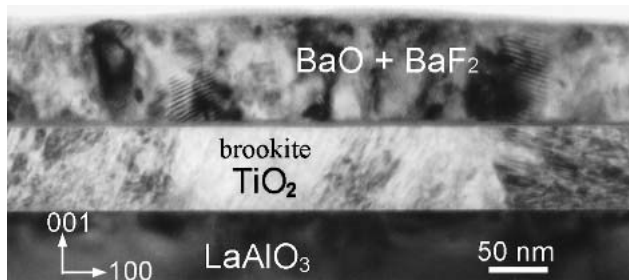


FIG. 3. Cross-sectional TEM image of the 400 °C annealed specimen.

Cross-sectional TEM specimens were prepared using the standard procedure of cutting, gluing, slicing, grinding, dimpling, and ion milling. The 200 °C annealed specimens were cooled during ion milling. TEM specimens were examined in a JEM 3010UHR (Japan) microscope by structural high-resolution imaging and by EELS using a Gatan post-microscope imaging filter. (Certain commercial equipment, instruments, or materials are identified in this paper to specify the experimental procedure adequately. Such identification is not intended to imply recommendation or endorsement by the National Institute of Standards and Technology, nor is it intended to imply that the materials or equipment identified are necessarily the best available for the purpose.) The high-resolution images were taken Scherzer defocus (−42 nm) at 300 kV. Medium-resolution electron micrographs were acquired with a Philips EM430. High-resolution and energy-filtered images were recorded with a charge-coupled device (CCD) camera and analyzed using the Gatan *Digital Micrograph* software package.

Energy-filtered images and EELS spectra were acquired on an FEI CM300FEG (Holland, The Netherlands) electron microscope equipped with a Gatan imaging filter and a Gatan multiscan CCD camera. The microscope was operated at 300 kV. Elemental maps were produced using the standard 3-window technique of combining energy-selected images (two pre-edge and one post-edge) with an empirically determined inverse power law background model. Images were registered manually for optimum drift correction, and the power law exponent was spatially smoothed before calculation of the

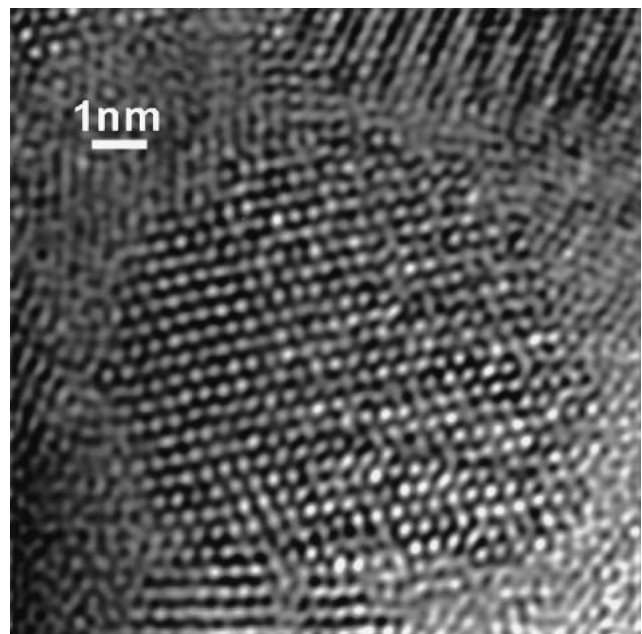


FIG. 4. [110] HREM image of a grain in the upper layer for the 400 °C annealed specimen.

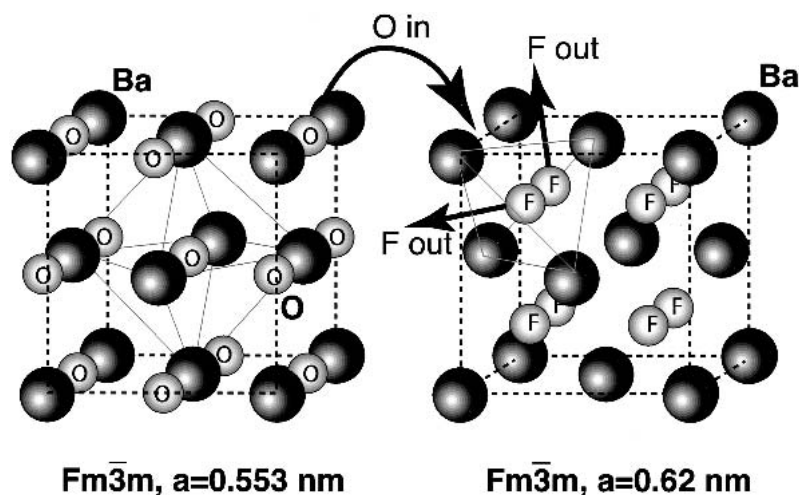


FIG. 5. Schematic drawing illustrating the proposed model of gradual substitution of F with O and change of the fluorite-type BaF<sub>2</sub> into BaO of rock salt structure.

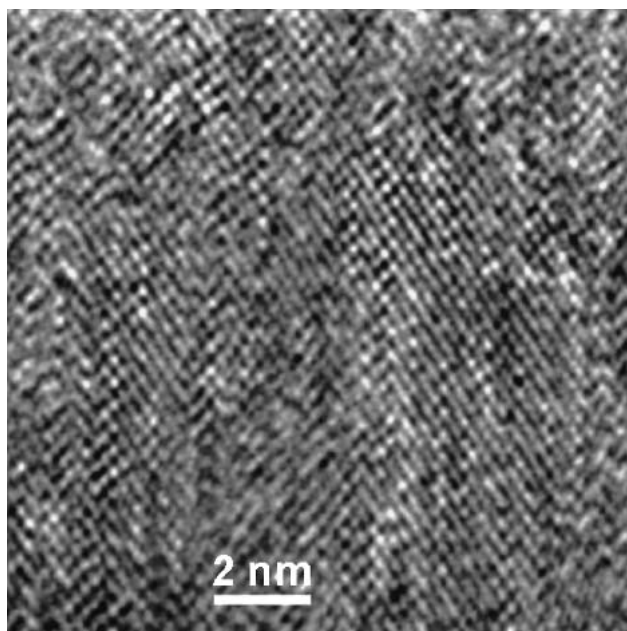
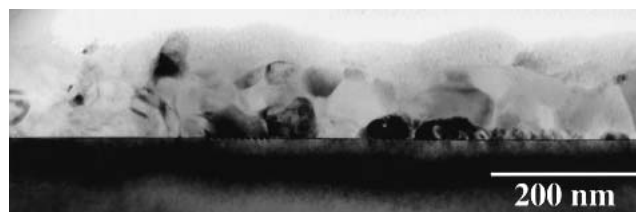


FIG. 6. HREM image of the Ti-O layer for the 400 °C annealed specimen. The observed structural contrast is interpreted as twinned TiO<sub>2</sub> (brookite) in [120] zone axis orientation.

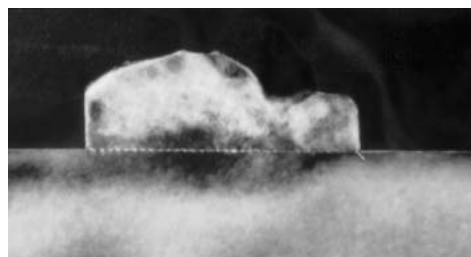
elemental maps. Because the images were acquired at relatively low magnification and spatial resolution was not a concern, relatively large slit widths were used during mapping to improve the core-loss EELS signal level. Titanium maps were made using the L<sub>2,3</sub> core-loss edge at 456 eV and a slit width of 30 eV. Barium maps were made using the M<sub>4,5</sub> core-loss edge at 781 eV and a slit width of 30 eV; the position of the Ba postedge window was adjusted to make optimal use of the white lines present in the Ba M edge and to minimize overlap with the nearby La M edge at 832 eV. EELS spectra were acquired for all samples prior to energy-filtered TEM.



(a)



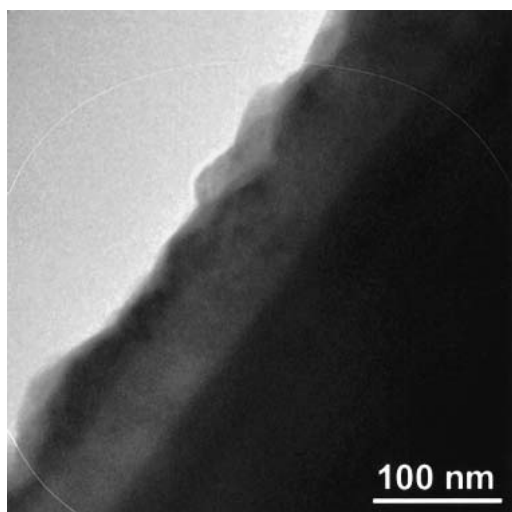
(b)



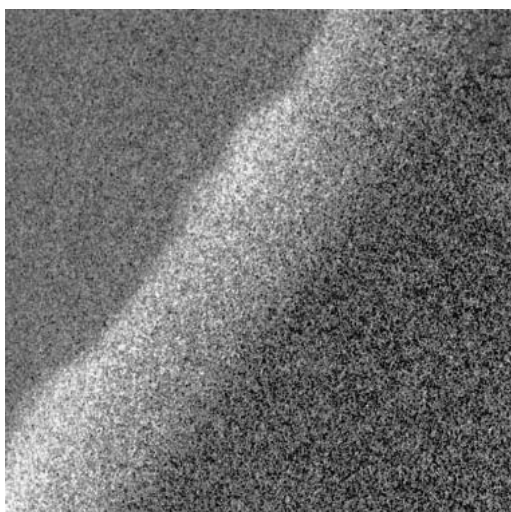
(c)

FIG. 7. Cross-sectional BF TEM image of the specimen heated from 400 to 700 °C: (a) bright-field imaging showing a polycrystalline structure; (b) dark-field imaging using close to each other reflections of the substrate and epitaxial BaTiO<sub>3</sub> perovskite. The image [see also an enlargement in (c)] shows islands of the epitaxial BaTiO<sub>3</sub>.

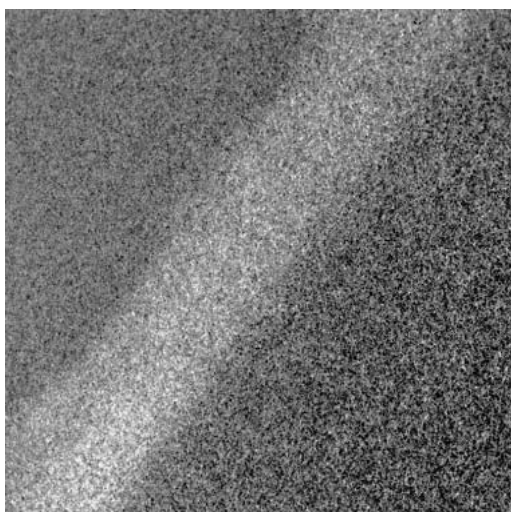
Confirmatory energy-dispersive x-ray spectra were acquired in scanning transmission electron microscopy (STEM) mode using an Oxford Link ISIS EDS detector (Oxford, UK), an XP-3 pulse processor, and an Emispec Vision data acquisition system.



(a)



(b)



(c)

FIG. 8. (a) Conventional bright-field micrograph of the specimen heated from 400 to 700 °C and EFTEM maps of the (b) Ba distribution and (c) Ti distribution made using the 3-window method.

### III. RESULTS AND DISCUSSION

The goal of this study was to understand the process of the mixing of the TiO<sub>2</sub> and BaF<sub>2</sub> precursor layers and the subsequent formation of BaTiO<sub>3</sub>. In the course of the investigation it became clear that the deposition process resulted in the occasional formation of regions where the ratio of TiO<sub>2</sub> to BaF<sub>2</sub> was significantly different from the targeted one. This is primarily the result of nonuniform delivery of BaF<sub>2</sub> caused by the formation of particulates, which is a typical problem of pulsed laser deposition. The particulate formation is especially pronounced in BaF<sub>2</sub> deposition because of the porosity and the brittle nature of the BaF<sub>2</sub> target used. These regions were easy to identify in the TEM. In the following discussion we present results for only those regions where the correct, uniform ratio of precursors was deposited.

#### A. Specimens annealed at 200 °C

Figure 1(a) shows a cross-sectional bright-field TEM image of the specimen annealed at 200 °C for 170 h. In this image the two precursor layers can be easily distinguished from each other. The bottom Ti–O layer, above the substrate and approximately 70-nm thick, shows uniform contrast typical of an amorphous structure and, therefore, corresponds to amorphous Ti–O. The top Ba–F layer, approximately 90-nm thick, shows the contrast of columnar crystalline grains. (The Ba–F thickness is less than the designed one, probably because of the high porosity of the BaF<sub>2</sub> target.) The layers have a sharp flat interface. According to the selected-area electron diffraction (SAED) pattern from the top layer [Fig. 1(b)] the grains are randomly oriented.

From the SAED pattern [Fig. 1(b)], we measured *d*-spacings of 0.36, 0.22, 0.14, and 0.126 nm (using reflections from the LAO substrate as an internal calibration). The measured values correspond reasonably well to a structure having a face-centered cubic lattice and *a* = 0.62 nm. High-resolution electron microscopy (HREM) provided a set of images from individual grains that supported this result. Figure 1(c) shows one such HREM image where two sets of orthogonal planes have the same spacing of approximately 0.3 nm corresponding to (200) planes and the [100] zone axis. A typical EELS spectrum from the top layer is shown in Fig. 2(a). In the 400- to 900-eV part of the spectrum, FK and BaL<sub>2,3</sub> edges can be clearly seen, as well as a weak O-K edge. The presence of the O-K edge indicates that the Ba–F layer has been partially oxidized during the prolonged annealing at 200 °C. We conclude that the structure of the grains is partially oxidized BaF<sub>2</sub> which in its bulk form has a fluorite *Fm* $\bar{3}$ *m* structure with lattice parameter *a* = 0.62 nm.

## B. Specimens annealed up to 400 °C

Figure 3 shows a cross-sectional TEM image of the specimen annealed at 400 °C for 24 h. The two precursor layers can still be distinguished by differences in contrast and by a relatively sharp interface. The upper layer (deposited Ba–F) has a polycrystalline contrast similar to the one seen in the 200 °C annealed specimens. Both  $d$ -values measured from SAED patterns and HREM images support cubic  $Fm\bar{3}m$  with  $a \approx 0.56$  nm. Figure 4 is an example of HREM showing a grain of the cubic structure in [110] orientation. The lattice parameter of the upper layer structure,  $a \approx 0.56$  nm, is significantly smaller than 0.62 nm of BaF<sub>2</sub>.<sup>7</sup> This lattice parameter corresponds well to the NaCl-type structure of BaO. According to the EELS spectra from the upper layer [Fig. 2(b)] it appears that the sample annealed at 400 °C has more O and less F relative to the sample annealed at 200 °C. On the basis of these results, we propose that, during annealing at 200 °C and then up to 400 °C, the as-deposited BaF<sub>2</sub> (fluorite structure) has changed into BaO (with a rock salt structure) by removal of F (from tetrahedral sites) and insertion of O into  $\langle 1/2\ 0\ 0 \rangle$  sites, as schematically shown in Fig. 5. It is not clear if the process is gradual or BaO<sub>*x*</sub>F<sub>2–2*x*</sub> reaches a solubility limit first and then BaO nucleates. According to the published BaO–BaF<sub>2</sub> eutectic phase diagram showing the two-phase equilibrium,<sup>8</sup> the solubility can be substantial.

It can also be seen from Fig. 3 that the bottom layer (deposited Ti–O) is no longer amorphous, since it exhibits diffraction contrast. Typical for this contrast are striations inclined to the LAO surface. These striations are apparently related to microtwin interfaces. Both SAED and HREM results demonstrated that the microtwin structure can be best explained as brookite—a polymorphic form of TiO<sub>2</sub>. Figure 6 shows such a HREM image in which the phase contrast is identified as that of TiO<sub>2</sub> brookite.<sup>7</sup> According to EELS mapping, only minor interdiffusion occurred between the Ti–O and Ba–O/F layers.

## C. Specimens heated to 700 °C

During the heating from 400 to 700 °C significant microstructural and compositional changes occurred. According to a bright field (BF) image, Fig. 7(a), both layers were transformed to a polycrystalline structure, and it is no longer possible to distinguish between the originally deposited layers. This microstructural change has been accompanied by apparently significant interdiffusion between the layers. Compositional EELS maps, Fig. 8, shows that at this stage significant mixing of Ba and Ti had occurred. However, some variations in composition have remained, and such nonuniformity resulted in the formation of Ba–Ti–O phases, which are in local

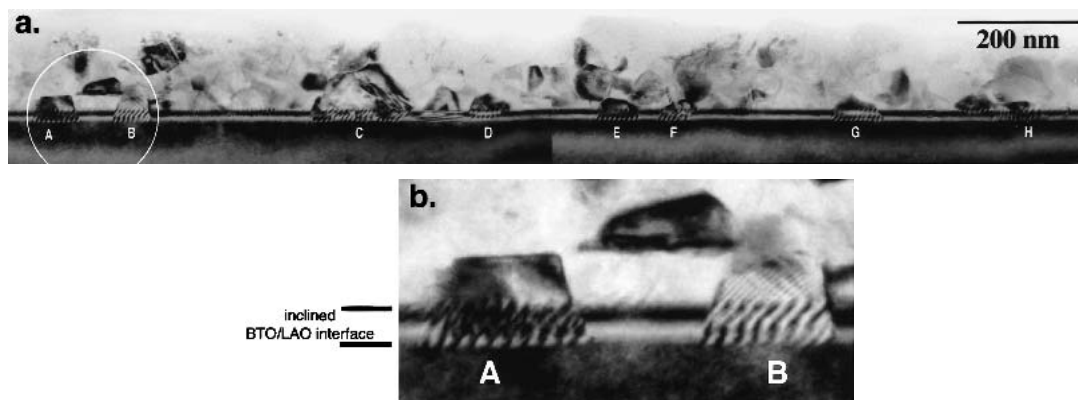


FIG. 9. Cross-sectional bright field TEM image of the specimen heated from 400 to 700 °C. The TEM specimen is tilted to show the substrate/film interface is strongly inclined to the electron beam direction. Along the interface the marked regions with Moiré fringes are nucleated grains of the epitaxial BaTiO<sub>3</sub> perovskite.

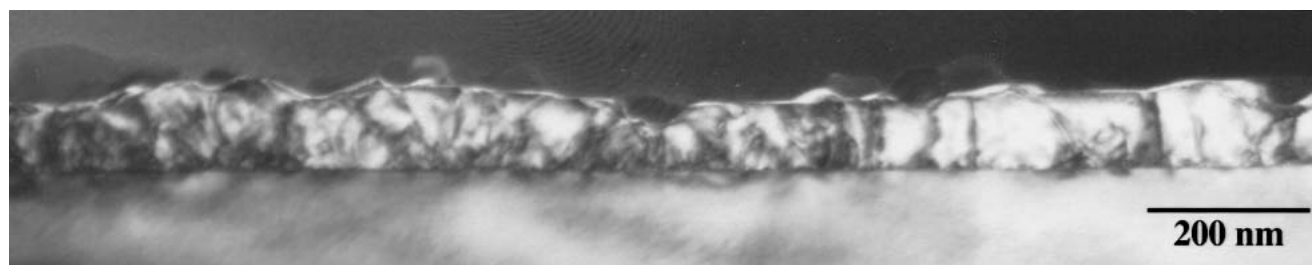
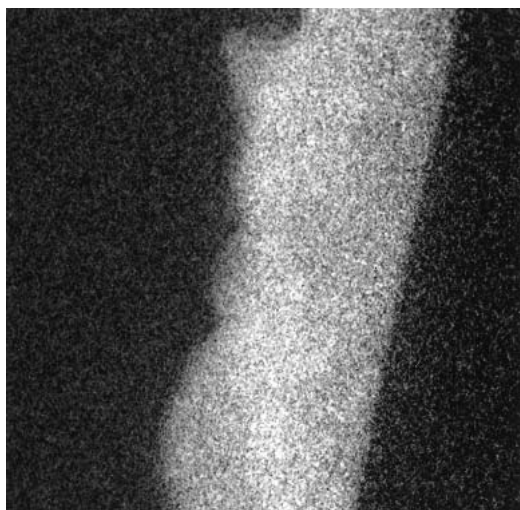


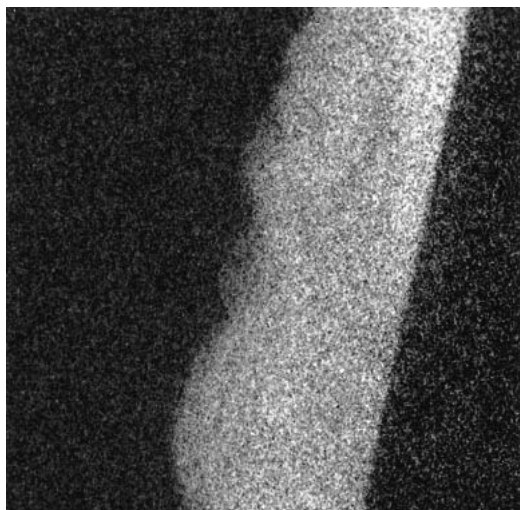
FIG. 10. Cross-sectional dark field TEM image of the specimen annealed at 900 °C for 1 h.



(a)



(b)



(c)

FIG. 11. (a) Conventional bright-field micrograph of the specimen annealed at 900 °C and EFTEM maps of the (b) Ba distribution and (c) Ti distribution made using the 3-window method.

equilibrium but are different from the cubic BaTiO<sub>3</sub> perovskite. Analysis of SAED and a number of microdiffraction patterns identified hexagonal BaTiO<sub>3</sub> and occasionally some other phases of the BaO–TiO<sub>2</sub> system, e.g., monoclinic BaTi<sub>2</sub>O<sub>5</sub>.<sup>9</sup>

Figure 7(b) shows a dark-field image complementary to the bright-field image in Fig. 7(a). The image was obtained using an objective aperture positioned over the (100) reflection of LAO. The bright contrast of some of the films grains, usually in contact with the substrate, suggests that those are the grains of the BaTiO<sub>3</sub> perovskite in epitaxial cube-to-cube orientation with the pseudocubic substrate. That assertion was confirmed by microdiffraction patterns obtained from these grains. Another visually appealing way of imaging these epitaxial grains is shown in Fig. 9. In this image the specimen is tilted in such a way that the substrate/film interface is strongly inclined to the electron beam direction. Along the interface most regions have contrast typical of an incoherent interface (broad thickness fringes), whereas in some part of the interface there are regions showing a set of dense fringes [e.g., A–H in Fig. 9(a)]. These dense fringes are Moiré fringes resulting from the interference between similar *g* vectors of the substrate and the epitaxial film. The observations demonstrate an early stage of formation of the epitaxial BaTiO<sub>3</sub> at 700 °C. Formation of the perovskite phase is promoted by structural compatibility with the substrate and the composition of the film approaching the phase stoichiometry.

#### D. Specimens annealed up to 900 °C

Figure 10 shows a cross-sectional dark-field TEM image [similar to that shown in Fig. 7(b)] of a film annealed at 900 °C for 1.5 h. A large continuous grain is seen. According to electron diffraction and dark-field imaging, the grain has a perovskite structure, which is in cube-to-cube orientation with the substrate. Some pockets of a polycrystalline structure could be also seen occasionally. (The structure is similar to that observed in the specimen annealed up to 700 °C.) Such a continuous film apparently resulted from the impingement of the epitaxial grains initially observed for the 700 °C specimen. The growth of the grains occurs both along the interface and upward, by consuming now metastable grains of the polycrystalline structure. Such a process is expected to generate structural defects, such as subgrain boundaries, dislocations, and stacking faults, all contributing to a mosaic spread.

Examination of an interface region reveals that the film has an atomically sharp interface with the substrate, without signs of interfacial reaction. Modulation of contrast along the interface, as seen in bright-field images, is a result of an elastic field of interfacial misfit

dislocations. The dislocations are periodically spaced, and the spacing is about 20 unit cells, which is consistent with near-complete relaxation of the lattice mismatch between LAO and BaTiO<sub>3</sub>. The spacing was estimated using expression  $D_{\delta} = (a_f + a_s)^2/[4(a_f - a_s)]$ ,<sup>10</sup> where  $D_{\delta}$  is the repeat distance between the misfit dislocations fully compensating misfit between the high-temperature LAO substrate ( $a_s = 0.3818$  nm) and the BTO film ( $a_f = .4046$  nm). Energy filtering transmission electron microscopy (EFTEM) maps of Ba and Ti of the sample (Fig. 11) show a homogeneous distribution, suggesting complete interdiffusion of these elements.

The present findings are consistent with an earlier investigation on similarly processed samples using Rutherford backscattering spectroscopy and x-ray diffraction that most significant diffusion and the compound crystallization take place at  $\geq 700$  °C.<sup>11</sup>

#### IV. CONCLUSIONS

PLD deposition of TiO<sub>2</sub> and BaF<sub>2</sub> layers and subsequent annealing were used to form homogeneous epitaxial BaTiO<sub>3</sub> films. In this paper we have investigated the microstructures of the films at different stages of the annealing using cross-sectional TEM, high-resolution imaging, energy-filtered imaging, and EELS spectroscopy. It was shown that large epitaxial BaTiO<sub>3</sub> grains could be formed on a LaAlO<sub>3</sub> substrate, and their formation process consisted of the following stages:

(1) At 200 °C, the microstructure of the precursors is believed to be very similar to the as-deposited structure. The TiO<sub>2</sub> layer is amorphous, as was previously suggested, and the BaF<sub>2</sub> layer is polycrystalline, with grains having a Ba fluorite structure and being partially oxidized.

(2) At up to 400 °C, the amorphous TiO<sub>2</sub> layer is crystallized to a microtwinned brookite structure, while further oxidation of BaF<sub>2</sub> and its transformation to BaO occurred. Early stages of interdiffusion are detected by EELS mapping.

(3) At up to 700 °C, significant interdiffusion has occurred, and the precursor layers have become almost indistinguishable. Overall, the structure of the film has become polycrystalline, with grains having a variation of different Ba–Ti–O phases corresponding to local equilibrium. Nucleation of the stable epitaxial perovskite BaTiO<sub>3</sub> on a substrate has been detected.

(4) At up to 900 °C, interdiffusion is completed, and epitaxial BaTiO<sub>3</sub> grains continue to nucleate and grow. Growth and impingement of BaTiO<sub>3</sub> result in consumption of polycrystalline, now metastable regions, and in the formation of a continuous epitaxial film.

The presence of off-stoichiometry polycrystalline regions in fully annealed films can be explained as (a) residual nonstoichiometric regions, not yet consumed by the recrystallization growth of BaTiO<sub>3</sub>, and (b) nonstoichiometric regions resulting from the inhomogeneous deposition of BaF<sub>2</sub>. The observations here further confirm the validity of the combinatorial precursor synthesis technique of creating compounds from amorphous precursors as applied to this material system. On the basis of the present results, we also believe that many other metal oxide systems (in particular perovskites) follow a similar evolution process starting from precursor layers.

#### ACKNOWLEDGMENTS

The authors acknowledge the assistance of R.L. Parke in TEM specimen preparation. We acknowledge support from the NSF [DMR 0094265 and Materials Research Science and Engineering Center (MRSEC)] at the University of Maryland.

#### REFERENCES

1. X-D. Xiang, X. Sun, G. Briceno, Y. Lou, K-A. Wang, H. Chang, W.G. Wallace-Freedman, S-W. Chen, and P.G. Schultz, *Science* **268**, 1738 (1995); G. Briceno, H. Chang, X. Sun, P.G. Schultz, and X-D. Xiang, *Science* **270**, 273 (1995); X-D. Xiang and P.G. Schultz, *Physica C* **282–287**, 428 (1997).
2. H. Koinuma, *Solid State Ionics* **108**, 1 (1998).
3. H. Chang, I. Takeuchi, and X-D. Xiang, *Appl. Phys. Lett.* **74**, 1165 (1999).
4. I. Takeuchi, H. Chang, C. Gao, P.G. Schultz, X-D. Xiang, R.P. Sharma, M.J. Downes, and T. Venkatesan, *Appl. Phys. Lett.* **73**, 894 (1998).
5. J. Wang, Y. Yoo, C. Gao, I. Takeuchi, X. Sun, H. Chang, X-D. Xiang, and P.G. Schultz, *Science* **279**, 1712 (1998).
6. H. Chang, C. Gao, I. Takeuchi, Y. Yoo, J. Wang, P.G. Schultz, X-D. Xiang, R.P. Sharma, M. Downes, and T. Venkatesan, *Appl. Phys. Lett.* **72**, 2185 (1998).
7. A.F. Wells, *Structural Inorganic Chemistry*, 5th ed. (Clarendon Press, Oxford, U.K., 1984).
8. T. Hara, *Tetsu to Do* **76**, 352 (1990) (in Japanese).
9. R.S. Roth, C.J. Rawn, C.G. Lindsay, and W. Wong-Ng, *J. Solid State Chem.* **104**, 99 (1993).
10. J.M. Howe, *Interfaces in Materials* (John Wiley & Sons, New York, 1997).
11. I. Takeuchi, K. Chang, L.A. Bendersky, H. Chang, X-D. Xiang, E.A. Stach, and C-Y. Song, *J. Appl. Phys.* (in press).